Endo- and Exocytosis of Zwitterionic Quantum Dot Nanoparticles by Live HeLa Cells

Xiue Jiang,[†,‡] Carlheinz Röcker,[‡] Margit Hafner,[‡] Stefan Brandholt,[†] René M. Dörlich,[†] and G. Ulrich Nienhaus[†,§,*]

[†]Institute of Applied Physics and Center for Functional Nanostructures (CFN), Karlsruhe Institute of Technology (KIT), Wolfgang-Gaede-Strasse 1, 76131 Karlsruhe, Germany, [‡]Institute of Biophysics, University of Ulm, Albert Einstein-Allee 11, 89081 Ulm, Germany, and [§]Department of Physics, University of Illinois at Urbana−Champaign, Urbana, Illinois 61801, United States

ABSTRACT Uptake and intracellular transport of D-penicillamine coated quantum dots (DPA-QDs) of 4 nm radius by live HeLa cells have been investigated systematically by spinning disk and 4Pi confocal microscopies. Unlike larger nanoparticles, these small DPA-QDs were observed to accumulate at the plasma membrane prior to internalization, and the uptake efficiency scaled nonlinearly with the nanoparticle concentration. Both observations indicate that a critical threshold density has to be exceeded for triggering the internalization process. By using specific inhibitors, we showed that DPA-QDs were predominantly internalized by clathrin-mediated endocytosis and to a smaller extent by macropinocytosis. Clusters of DPA-QDs were found in endosomes, which were actively transported along microtubules toward the perinuclear region. Later on, a significant fraction of endocytosed DPA-QDs were found in lysosomes, while others were actively transported to the cell periphery and exocytosed with a half-life of 21 min.

KEYWORDS: quantum dots · endoytosis · exocytosis · live-cell imaging · uptake mechanism · uptake inhibition · confocal microscopy

Nanotechnology is a rapidly advancing field, and an ever increasing array of engineered nanoparticles are finding their way into diverse industrial applications. This development inevitably entails an enhanced likelihood of human exposure to engineered nanoparticles. Owing to their small size, nanoparticles can penetrate physiological barriers, translocate, and accumulate in living organisms, and there is growing concern that exposure to certain types of nanoparticles may have significant adverse health effects.[1] Therefore, a profound knowledge of the interactions of nanoparticles with living organisms is a prerequisite for the safe use of nanotechnology to reap its potential benefits while limiting the associated health hazards.

Owing to their small size (diameter <100 nm), nanoparticles are incorporated by cells *via* endocytosis, a process that enables cells to ingest materials such as proteins that cannot penetrate the plasma membrane. Endocytosis of biomacromolecules and viruses has been investigated for many years.[2,3] More recently, nanoparticles have been employed as model cargoes to study endocytosis mechanisms[4,5] because their size, shape, surface charge, and surface decoration with functional groups can be finely tuned at the atomic scale. We also note that surface properties govern adsorption of proteins to nanoparticle surfaces, which occurs when nanoparticles come into contact with biological fluids in the organism.[6,7] Detailed investigations of the relationships between the physicochemical properties of nanoparticles and the elicited cellular uptake activity are a prerequisite to understand and control these interactions.[8−16]

Luminescent nanoparticles allow one to visualize the uptake process and track cargo within the cell using optical microscopy. Owing to their small size (diameter 1−5 nm), brightness, and photostability, colloidal semiconductor core/shell quantum dots (QDs) hold great promise for applications in biotechnology and biomedicine,[17,18] especially *in vivo* imaging[19,20] and cellular tracking.[21−24] After synthesis, these nanocrystals are insoluble in aqueous media. To make them suitable for biological applications, they have to be rendered soluble and colloidally stable in physiological solvents by coating their surfaces with hydrophilic groups. A range of solubilization procedures have been established that however increase the nanoparticle size to varying extents.[25] Water-soluble, thiolated molecules are among the most commonly used ligands for this purpose.[26] Recently, we have shown that CdSe/ZnS core/shell QDs

*Address correspondence to uli@illinois.edu.

Received for review June 7, 2010 and accepted October 18, 2010.

Published online October 28, 2010. 10.1021/nn101277w

© 2010 American Chemical Society

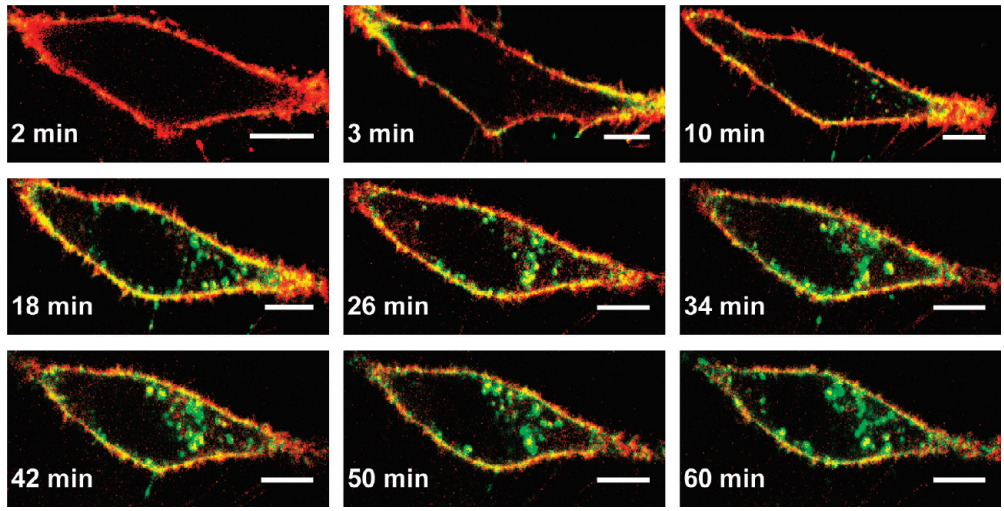

Figure 1. Time sequence of merged two-color confocal images of a HeLa cell exposed to DPA-QDs (green) for different times. The plasma membrane was stained with the red membrane dye CellMask Deep Red (red). The experiment was performed under live cell conditions (5% CO_2, 37 °C) using a DPA-QD concentration of 10 nM. Scale bar: 10 μm.

coated with the small, zwitterionic thiol ligand D-penicillamine (DPA-QDs) feature much improved colloidal stability in physiological media over the popular 11-mercaptoundecanoic acid-coated QDs.[27] The small DPA ligand adds minimally to the overall size of the nanoparticle, and DPA-QDs resemble small protein molecules with regard to size, near-neutral charge, and functional groups (amine and carboxylic acid groups). In this work, we have investigated endocytosis and intracellular processing of DPA-QDs in detail.

Endocytosis encompasses several distinct active cellular mechanisms, which provide cells with the ability to internalize nutrients including macromolecules and larger particles. In general, the preference for a particular mechanism depends on the cell type. Phagocytosis, the process by which larger particles are taken up, is carried out by specialized cells, so-called phagocytes, whereas pinocytosis of particles ranging from a few to up to a few hundred nanometers occurs in virtually all cells and is crucial for intercellular communication and nutrient uptake. Four basic pinocytosis mechanisms are being distinguished: macropinocytosis, clathrin- or caveolae-mediated endocytosis, and mechanisms that neither involve clathrin nor caveolae.[3] A variety of inhibitors are known that selectively suppress certain pathways, so that the relevance of one mechanism over another can be studied.[28−30] Clathrin-dependent endocytosis is probably the best characterized uptake mechanism, in which cargo is deposited in small endocytic vesicles (diameter ≈ 100 nm) that fuse with early endosomes. In these organelles, cargo is sorted either for recycling to the cell surface or further processing in late endosomes or lysosomes.[31]

Previous studies of endocytosis of nanoparticles have focused on static techniques;[8,9,32−34] detailed investigations of uptake kinetics are still scarce.[21,22] Here we have used spinning disk and 4Pi confocal fluorescence microscopy techniques to visualize the interaction of small, zwitterionic QDs with cultured HeLa cells under live-cell conditions. The experiments were carried out in buffer solutions rather than in cell culture media to avoid specific effects of serum proteins, which are known to interact with the nanoparticles and receptors on the plasma membrane and can, thereby, markedly influence nanoparticle uptake. Although optical microscopy offers only limited resolution as compared to transmission electron microscopy, it has the key advantage that it allows nanoparticle interactions with living cells to be studied in real time. Thus, we have been able to measure the kinetics of particle uptake, distinguish cell membrane association from cellular incorporation, analyze uptake pathways, and observe trafficking of the nanoparticles to subcellular compartments.

RESULTS

HeLa Cell Exposure to DPA-QDs. To observe binding of DPA-QDs to live HeLa cells and their subsequent internalization, we incubated cells with PBS solutions containing 10 nM DPA-QDs. These nanoparticles, which were characterized thoroughly in an earlier paper,[27] have a radius of ∼4 nm and a zeta potential of −40 mV. Spectra and fluorescence images of these nanoparticles are included as Supporting Information (Figure S1). We imaged the cells during DPA-QD exposure for typically 1 h by using spinning disk confocal microscopy with detection in two separate spectral channels. Figure 1 shows, as an example, fluorescence images for selected times after QD exposure. Membranes and DPA-QDs are depicted in red and green, respectively, so that colocalization of membrane dye and DPA-QDs is seen in yellow color in the overlay image. DPA-QDs appeared at the cell membrane within 1 min after incubation and gradually accumulated there afterward. Inside the cell, however, the first few small bright spots appeared

near the cell periphery 3 min after incubation. Subsequently, more and more DPA-QDs were internalized by the cell and transported to the perinuclear region, where they formed large clusters within 1 h of incubation. Although the membrane dye, which primarily stains the plasma membrane and vesicles derived from the plasma membrane,[35] bleaches significantly during the experiment, many yellow-green dots are present in Figure 1, which indicates colocalization of DPA-QDs and membrane dye. This observation suggests that the internalized DPA-QDs are trapped in endosomal vesicles.

We also studied the response of live HeLa cells to different concentrations of DPA-QDs. Confocal images after 1 h incubation with 10, 3, and 1 nM DPA-QDs, respectively, are shown in Figure 2a−c. Obviously, the amount of DPA-QDs both at the plasma membrane and inside the cell was lowered with decreasing particle concentration. At 1 nM DPA-QDs, only very few nanoparticles were observed in the interior of the cells. We obtained information about the membrane-associated and internalized fractions by quantitative image analysis. In Figure 2d, the integrated fluorescence intensity, normalized to the cross sectional area in the observation plane, is shown separately for the plasma membrane and the cell interior. This quantity captures the fluorescence intensity of all particles contributing within the spectral window including those that escape detection as individual spots.

At 10 nM DPA-QD concentration, about equal amounts of nanoparticles were associated with the cell membrane and within the cells after 1 h. With decreasing nanoparticle concentration, however, the intracellular fraction decreased much more strongly than the membrane-associated part. This result was further supported by kinetic analysis (Figure 2e). The membrane-associated fraction (upper panel) saturated on the hour time scale, whereas the intracellular fraction (lower panel) increased approximately linearly in time. The uptake rate (slope in panel e) scales nonlinearly with the QD concentration; it is ~5-fold lower at 3 nM (blue dots) and ~30-fold lower at 1 nM (red dots) than at 10 nM DPA-QDs (black dots). Consequently, internalization of small DPA-QDs of 4 nm radius depends strongly on the amount of nanoparticles binding to the cell membrane. At a concentration of 10 nM DPA-QDs, strong accumulation on the membrane within the first few minutes was accompanied by fast, continuous internalization of nanoparticles, whereas internalization of nanoparticles was barely detectable after 1 h exposure to 1 nM DPA-QD solutions.

Mechanisms Involved in the Internalization of DPA-QDs by HeLa Cells. To gain insight into the relative importance of the different endocytosis pathways of HeLa cells, we studied the effect of inhibitors that interfere with particular uptake mechanisms. Representative confocal images are shown in Figure 3a−d. Dynasore acts as a specific inhibitor of endocytic pathways that depend on the protein dynamin,[36] a large GTPase forming a helix around the neck of a nascent endocytic vesicle. GTP hydrolysis results in an axial extension of this helix, cleaving the vesicle's neck from the parent membrane. Application of dynasore to cells suppresses the function of dynamin and, consequently, all dynamin-dependent endocytosis pathways, including clathrin- and caveolin-mediated endocytosis. Comparison of DPA-QD uptake in the absence (Figure 3a) and presence (Figure 3b) of dynasore reveals that internalization is strongly suppressed by dynasore. However, membrane association is hardly affected. These observations are corroborated by the quantitative analyses in Figure 3e,f. In the control experiment (Figure 3e), about half of the nanoparticles were internalized by the cells, and the other half were associated with the cell membrane. After the addition of dynasore, we found that internalization of DPA-QDs was significantly suppressed to ~30%, whereas the membrane-associated part was not affected at all (Figure 3f). Therefore, we conclude that ~70% of the DPA-QDs are internalized *via* a dynamin-dependent pathway. To further clarify the internalization mechanism, we also applied chlorpromazine to the cells (Figure 3c), a cationic, amphiphilic drug that inhibits clathrin assembly at the plasma membrane.[37] Clathrin forms a polyhe-

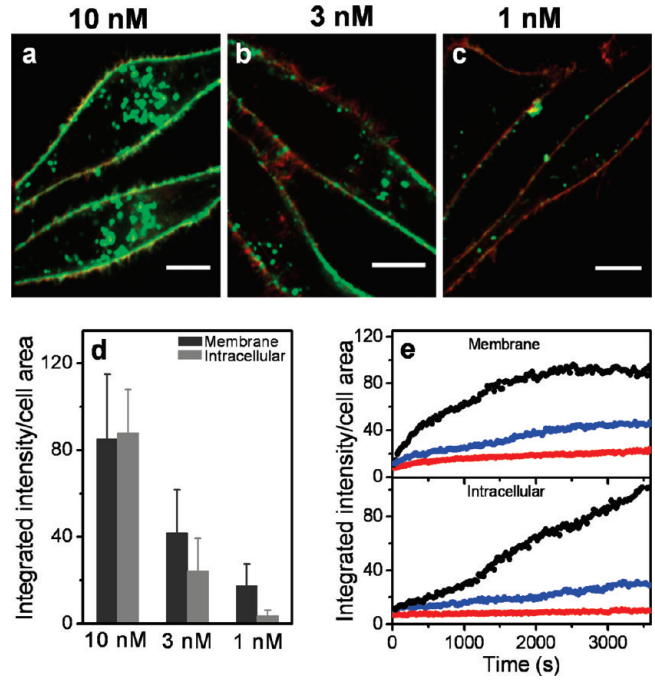

Figure 2. Dose-dependent uptake of DPA-QDs by HeLa cells. Confocal images of HeLa cells after 1 h exposure to PBS solutions containing DPA-QDs at concentrations of (a) 10, (b) 3, and (c) 1 nM. Scale bar: 10 μm. (d) Dose-dependent uptake of DPA-QDs by HeLa cells after 1 h incubation, as determined by quantitative analysis of membrane associated (dark gray bar) and intracellular (light gray bar) fluorescence. Results are averages of three different experiments with altogether 15 cells. (e) Kinetics of nanoparticle association with HeLa cells at 10 (black), 3 (blue), and 1 nM (red) DPA-QDs. Membrane-associated (upper panel) and intracellular (lower panel) regions were analyzed separately for 3−6 cells each in three different experiments.

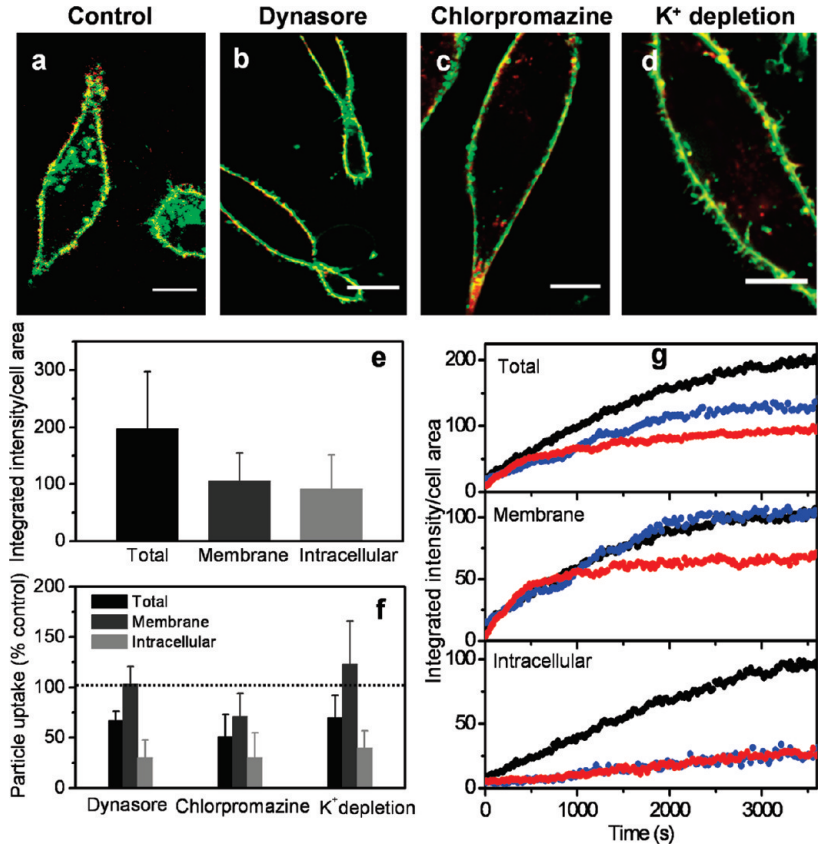

Figure 3. Effect of inhibitors on the uptake of DPA-QDs by HeLa cells. Confocal images of HeLa cells after 1 h incubation with 10 nM DPA-QDs (a) without inhibitor (control), in the presence of (b) dynasore, (c) chlorpromazine, and (d) under K^+ depletion. Scale bar: 10 μm. (e) Total uptake of DPA-QDs by HeLa cells after 1 h incubation, as determined by quantitative image analysis (black bar) and separation into membrane-associated (dark gray bar) and internalized nanoparticles (light gray bar). (f) Effect of inhibitors on the uptake of DPA-QDs by HeLa cells, averaged from 15 cells in three different experiments. (g) Effect of dynasore (blue) and chlorpromazine (red) on the uptake kinetics of DPA-QDs by HeLa cells relative to control (black). Total uptake (upper panel), membrane-associated (middle panel), and internalized fraction (lower panel) were analyzed separately. Kinetic traces are averages from 3 to 6 cells in three different experiments.

dral lattice that coats the endocytic vesicle. Addition of chlorpromazine not only significantly suppressed the internalization of DPA-QDs to 30% but also suppressed the membrane-associated part (70%) (Figure 3f). Comparing the extent of suppression of internalized DPA-QDs induced by dynasore and chlorpromazine, we conclude that internalization of DPA-QDs occurs predominantly *via* clathrin-dependent endocytosis. To further strengthen this conclusion, we also examined uptake of DPA-QDs under conditions of potassium depletion (Figure 3d), which also interferes with receptor-mediated endocytosis by arresting clathrin-coated pit formation.[2,28] Potassium depletion was found to result in a suppression of nanoparticle internalization highly consistent with that induced by chlorpromazine (Figure 3).

The effect of dynasore (blue dots) and chlorpromazine (red dots) on the kinetics of DPA-QD uptake is compared with the control experiment (black dots) in Figure 3g. The kinetics of membrane association was hardly affected by the inhibitors, particularly during the first 1000 s (Figure 3g, middle panel); only the saturation level was a bit lower for chlorpromazine. However, internalization of DPA-QDs was almost completely blocked during the first ~800 s after incubation in the presence of either chlorpromazine or dynasore (Figure 3g, lower panel), and, subsequently, a similar increase of the intracellular population, approximately linear in time, was observed. These findings lend further credence to our claim that endocytosis of DPA-QDs occurs mainly by a clathrin-mediated mechanism.

We used 4Pi confocal imaging, a technique that offers ~5-fold better axial resolution (~100 nm) than conventional confocal microscopy,[38] to investigate structural changes at the plasma membrane upon interaction with DPA-QDs and inhibitors. Quite different effects were observed in the presence of dynasore (Figure 4a–c) and chlorpromazine (Figure 4d–f). With dynasore, we observed extensive colocalization of membrane structures and nanoparticles (Figure 4c, white arrow), whereas such an effect was absent with chlorpromazine (Figure 4f). These observations can be understood on the basis of the different effects by which these two drugs suppress nanoparticle internalization. Chlorpromazine disturbs membrane invagination and vesicle formation, and therefore, nanoparticle

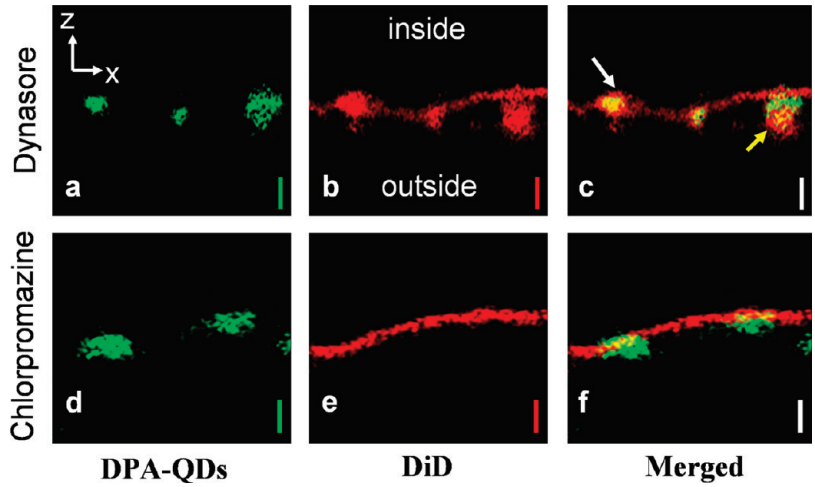

Figure 4. 4Pi confocal images of HeLa cell membranes in the presence of DPA-QDs and inhibitors. Cells were incubated for 1 h with 10 nM DPA-QDs (green) in the presence of dynasore (a−c) or chlorpromazine (d−f). The plasma membrane was stained with DiD (red). Scale bar: 0.5 μm.

clusters are retained at the cell surface. Dynasore does not suppress invagination and wrapping of nanoparticles but inhibits dynamin action and, thereby, prevents the release of completely formed clathrin-coated pits into the cytosol. In Figure 4c (yellow arrow), a spot is seen that stands outside of the cell that may represent a macropinocytosis vesicle. To verify the involvement of macropinocytosis to the internalization of DPA-QDs, 5-(*N*-ethyl-*N*-isopropyl)amiloride (EIPA) was applied to the cells, which inhibits macropinocytosis by specific inhibition of the Na^+/H^+ antiporters in the cell membrane.[30,39,40] Quantitative analysis of spinning disk microscopy images revealed a suppression of DPA-QD internalization by ~25% (Supporting Information, Figure S2), implying that macropinocytosis also plays a significant role in the uptake of DPA-QDs. We further inspected a large number of fixed HeLa cells that had been exposed to nanoparticles after EIPA treatment by using 4Pi confocal imaging. We failed to observe a feature such as the one in Figure 4c (yellow arrow) under these conditions.

Active Transport and Processing of Internalized DPA-QDs. We tracked the motions of endocytosed DPA-QDs within the cells by time-lapse acquisition of images every 3 s. Most bright green objects, which correspond to nanoparticle-loaded vesicles, translocated from the cell periphery to the perinuclear region in a steady motion. Such a behavior is expected for active vesicle transport by motor proteins along microtubules. Figure 5a shows a typical trajectory together with the analysis of the distance traveled (Figure 5b, black squares) and the corresponding velocity (Figure 5c, black squares) as a function of time. In Figure 5b and c, data from other trajectory analyses are also included in different colors. Active transport proceeded for a few micrometers until the vesicles stalled or disappeared, either due to detachment of the motors from microtubules or, possibly, escape of the vesicle from the focal plane. The transport velocities ranged from 0 − 0.4 μm/s (Figure 5d, cyan distribution). The average velocity of 0.27 ± 0.07 μm/s is lower than the reported velocities of (0.7 ± 0.07 μm/s)[41] for dynein-mediated active transport *in vitro* and the values for active transport of peptide-conjugated QDs in HeLa cells (~1 μm/s)[35,42] but consistent with transport velocities of melanosomes[43] and QD-receptor complexes[23] in living cells. Evidently, the velocity of active DPA-QD transport in HeLa cells depends on the availability of ATP. In our experiments, the cells were immersed in PBS solution, so that the ATP concentration and, concomitantly, the velocity of active transport must decrease over time for lack of nutrients. Indeed, if the HeLa cells were starved by incubating with PBS for 1 and 3 h prior to nanoparticle application, the (average) velocities decreased to 0.25 ± 0.06 (Figure 5d, gray bars) and 0.20 ± 0.04 μm/s (Figure 5d, pink bars), respectively.

After ~1 h of incubation with DPA-QDs, more and more loaded vesicles were observed to migrate back to the cell periphery (Figure 6a). Distances traveled and the corresponding velocities are shown as a function of time in Figure 6 panels b and c, respectively. These velocities range from 0.1−0.3 μm/s, the average is 0.23 ± 0.05 μm/s (Figure 6d, cyan bars). If the HeLa cells were preincubated with PBS for 1 or 3 h prior to the incubation with DPA-QDs, the average velocities were lower, 0.21 ± 0.06 (gray bars) and 0.19 ± 0.06 μm/s (pink bars), respectively, as expected due to ATP depletion.

To further characterize the transport mechanism, we preincubated HeLa cells with the cytoskeleton-disrupting drugs nocodazole and cytochalasin D. Application of the microtubule-disrupting nocodazole led to a reduced presence of DPA-QDs inside the cell, especially in the perinuclear region (Figure 7a). Quantitative image analysis revealed a reduction of uptake by two-thirds (Figure 7c); membrane association of nanoparti-

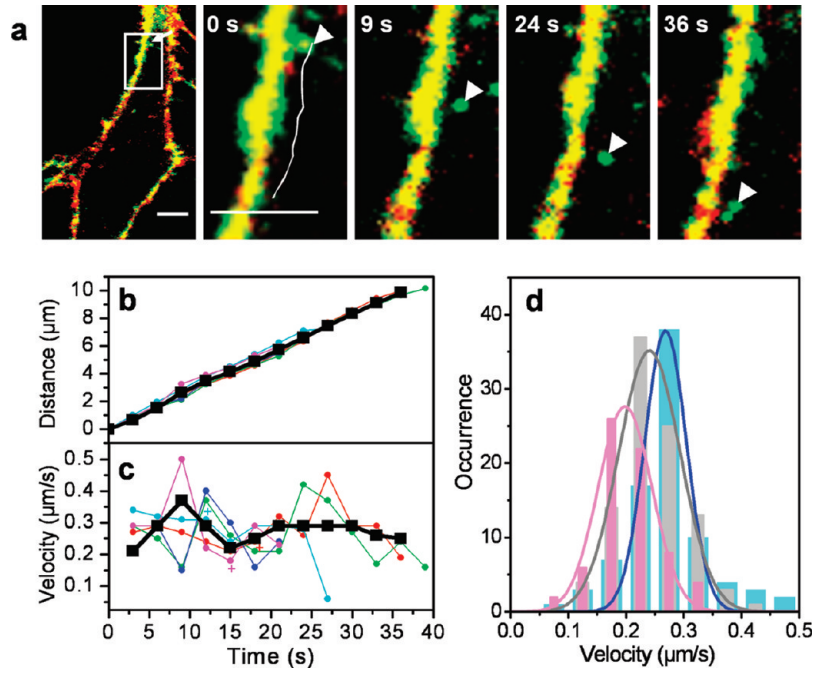

Figure 5. Active transport of DPA-QD loaded vesicles inside live HeLa cells from the cell periphery to the perinuclear region. (a) The area marked by the white box in the first image is expanded in a time series showing the movement of a vesicle. The trajectory is marked by a white line in the first expanded image (scale bar: 5 μm). (b) Distance and (c) velocity *versus* time diagrams for several DPA-QD vesicles moving from the cell periphery toward the nucleus. The black squares represent data from the vesicle shown in panel a. A few data points are marked with "+" to indicate transport in the reverse direction. (d) Histogram of (forward) velocities after preincubation with PBS for 5 min (cyan bars), 1 h (gray bars), and 3 h (pink bars).

cles was affected only to a lesser extent. In the presence of nocodazole, the trajectories of DPA-QD loaded vesicles exhibited frequent pauses and direction reversals (Figure 7d). These observations indicate that DPA-QD loaded vesicles were transported from the periphery to the perinuclear region by microtubule-based dyneins.[41] Application of cytochalasin D, which inhibits F-actin polymerization, led to strong suppression of DPA-QD internalization, which is apparent from confocal images (Figure 7b) and their quantitative analysis (Figure 7c). The pronounced effect of cytochalasin D on DPA-QD uptake underscores the key role of the actin cytoskeleton in the endocytic machinery.[44]

To gain information about the fate of internalized DPA-QDs within HeLa cells, DPA-QDs were co-incubated with labeled transferrin (Figure 8a−c). Transferrin is internalized *via* clathrin-mediated endocytosis[15] and widely used as an endosomal marker. Similar patterns are observed upon staining with DPA-QDs (Figure 8a) and fluorescently labeled transferrin (Figure 8b). The yellow spots in the merged image (Figure 8c) reveal extensive colocalization, which shows that the internalized DPA-QDs reside within endosomes. We also incubated HeLa cells with DPA-QDs and LysoTracker, a specific marker of lysosomes. In images taken 1.5 h after nanoparticle exposure (Figure 8d−f), colocalization with LysoTracker is clearly visible from the yellow spots in the merged image (Figure 8f), showing that the internalized DPA-QDs also end up in lysosomes.

To study exocytosis of internalized DPA-QDs, HeLa cells were first exposed to 10 nM DPA-QD solution for 1.5 h. Subsequently, the cells were washed and incubated with fresh cell medium. A time series of *z*-stacks was recorded with the spinning-disk confocal microscope. The loss of the intracellular nanoparticle population after solution exchange was analyzed to yield the exocytosis kinetics (Figure 8g). The exocytosed fraction increased with a half-life of 21 min and reached saturation after ~2 h. A little more than half the initially internalized DPA-QDs were again expelled by the cells.

DISCUSSION AND CONCLUSIONS

We have investigated the interaction of small DPA-QDs of 4 nm radius with live HeLa cells, including their binding to the cell membrane, mechanisms of internalization, trafficking within the cell and exocytosis (Figure 9). The brightness and photostability of DPA-QDs greatly facilitated our long-term observations. A substantial fraction of the cellular fluorescence is due to nanoparticles that are not internalized but only attached to the cell membrane. In this case, fluorescence imaging offers clear advantages over techniques that integrate over entire cells such as fluorescence-assisted cell sorting (FACS).[13]

The majority of DPA-QD nanoparticles were endocytosed *via* the clathrin-mediated pathway, as seen from the suppression of internalization by almost 70% upon dynasore and chlorpromazine application or depletion

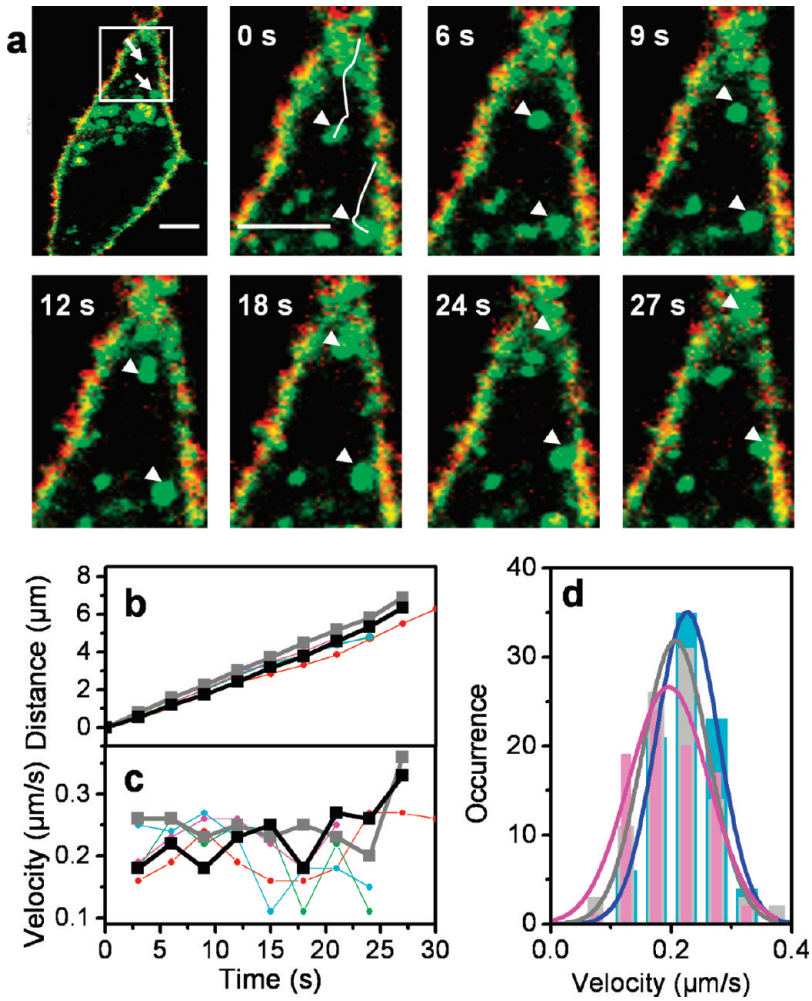

Figure 6. Active transport of DPA-QD loaded vesicles inside live HeLa cells toward the cell periphery. (a) The area marked by the white box in the first image is expanded in a time series movement of two vesicles. The trajectories are marked by white lines in the first expanded image (scale bar: 5 μm). (b) Distance and (c) velocity *versus* time diagrams for several DPA-QD vesicles. The black and gray squares represent data from the two examples shown in panel a. (d) Histogram of velocities for experiments with preincubation with PBS for 5 min (cyan bar), 1 h (gray bar), and 3 h (pink bar).

of intracellular K^+. Clathrin-mediated endocytosis is additionally supported by colocalization of the internalized DPA-QDs with fluorescently labeled transferrin, a classic marker of clathrin-mediated endocytosis. Unlike dynasore or K^+ depletion, both of which do not affect binding to the cell membrane, application of chlorpromazine weakly decreases the amount DPA-QDs on the cell membrane. This observation may be related to the known effect of chlorpromazine, which suppresses the formation of clathrin-coated pits on the cell surface. Thus, reduced nanoparticle binding may result from the overall smaller surface area of the plasma membrane. The pronounced difference in the plasma membrane structure upon application of dynasore and chlorpromazine is obvious from the high resolution 4Pi confocal images (Figure 4). A smaller fraction of DPA-QDs enters the cells *via* macropinocytosis, as shown by application of the specific inhibitor EIPA and further supported by 4Pi confocal imaging of nanoparticle-membrane structures that may represent macropinocytosis vesicles (Figure 4).

The observed accumulation of DPA-QDs on the cell membrane (Figure 1) differs dramatically from results obtained with larger nanoparticles (radius ≈ 50 nm) internalized by living cells, which were also internalized by clathrin-mediated endocytosis but did not at all accumulate on the cell membrane.[13] In general, internalization is initiated by nanoparticle binding to receptors in the cell membrane, which then trigger the assembly of cytoskeletal structures that generate the force required to locally wrap the membrane around the nanoparticle.[45] Once a nanoparticle attaches to the membrane, more and more receptors diffuse into the binding site and bind to the nanoparticle, so that the membrane wraps around the nanoparticle. This process continues until the nanoparticle is entirely engulfed by the membrane. Receptor-mediated endocytosis strongly depends on the nanoparticle size; the optimal radius was reported to be ~25 nm.[5,46] For very small nanoparticles such as our DPA-QDs with a radius of 4 nm, complete wrapping can only occur if a sufficiently large cluster of nanoparticles are packaged in one

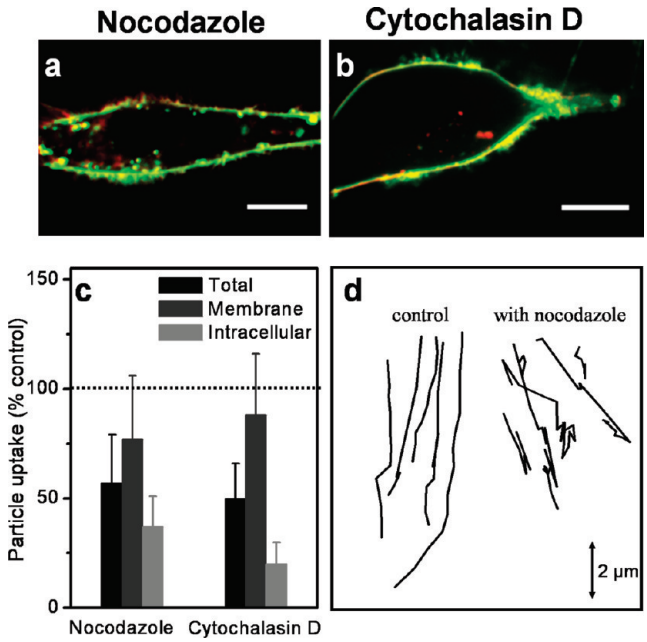

Figure 7. Inhibition of DPA-QD endocytosis by cytoskeleton-disrupting drugs. Confocal images of HeLa cells after 1 h incubation with 10 nM DPA-QDs and (a) nocodazole and (b) cytochalasin D (scale bar: 10 μm). (c) Effect of nocodazole and cytochalasin D on the uptake of DPA-QDs by HeLa cells after 1 h incubation, as determined by quantitative image analysis. (d) Sample trajectories for several DPA-QD loaded vesicles in HeLa cells in the absence (control) and presence of nocodazole.

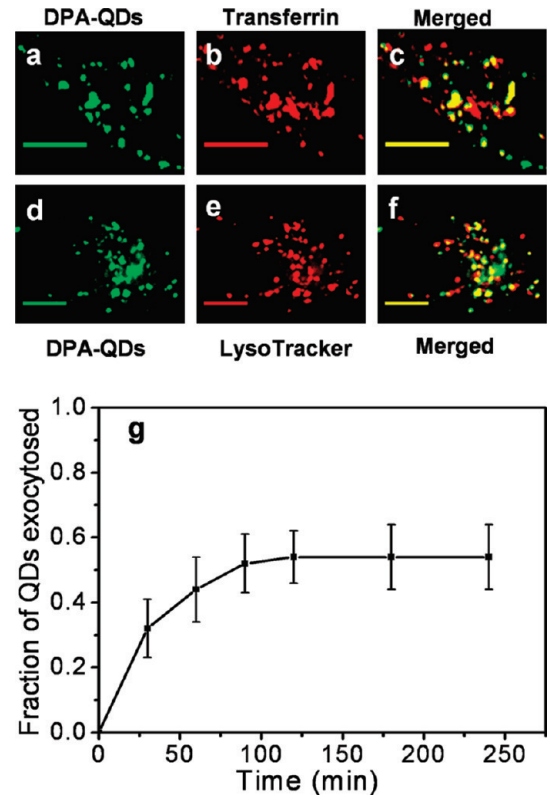

Figure 8. Intracellular fate of internalized DPA-QDs. (a−c) HeLa cells were incubated with AlexaFluor 647 labeled transferrin for 30 min, washed, and incubated with DPA-QDs for another 40 min. Green and red spots show the intracellular distribution of DPA-QDs and transferrin-containing endosomes, and the yellow spots in the merged image indicate colocalization of DPA-QDs with endosomes. (d−f) HeLa cells were incubated with 10 nM DPA-QDs for 30 min, washed, incubated with the lysosomal marker LysoTracker Green DND 26 for another 1 h. Green and red spots show the intracellular distribution of DPA-QDs and lysosomes, and the yellow spots in the merged image indicate colocalization of DPA-QDs and lysosomes. (g) Kinetics of exocytosis of DPA-QDs after replacing the external solution by cell medium.

vesicle. In our previous experiments,[13] large nanoparticles were not observed at the cell membrane. Apparently, receptor diffusion is sufficiently fast so that complete wrapping occurs within less than a second. Small nanoparticles, however, first attach to the cell membrane but then they cannot be taken up individually. Only if a critical density is reached locally, can wrapping of an entire cluster proceed to completion. This conclusion is further supported by the dose-dependent uptake experiments shown in Figure 2. Whereas the membrane-associated fraction scaled with the nanoparticle concentration within the experimental error, the amount of internalized nanoparticles decreased much more strongly, and at 1 nM DPA-QD concentration, internalization was barely observed during 1 h of incubation.

Internalized DPA-QDs were found trapped in endosomes, which were actively transported along microtubules, as verified by treatment of the cells with nocodazole (Figure 7). DPA-QD loaded vesicles were actively transported from the periphery to the perinuclear region by dynein motors, with typical trajectory lengths of >3 μm. A significant fraction of internalized DPA-QDs was found to end up in lysosomes (Figure 6), but about one-half of the DPA-QDs were actively transported to the periphery and again excreted by the cells, as shown by kinetic experiments after uptake saturation.

METHODS

Nanoparticle Preparation and Characterization. DPA-QDs were prepared as previously reported.[27] Briefly, CdSe/ZnS core/shell QDs were synthesized in organic solvent prior to ligand exchange with DPA, yielding watersoluble zwitterionic nanoparticles. The fluorescence emission spectrum of the DPA-QDs showed a peak at 591 nm (SPEX Fluorolog II, Horiba Jobin Yvon, Edison, NJ); a hydrodynamic radius of (4.0 ± 0.3) nm was determined by fluorescence correlation spectroscopy using a home-built setup.[7] The zeta potential of the DPA-QDs was determined at 25 °C by using a Malvern Zetasizer Nano ZS (Worcestershire, UK).

Live Cell Confocal Imaging. HeLa cells were cultured in Dulbecco's modified eagle medium (DMEM), supplemented with 10% fetal bovine serum, 100 U of penicillin, and 100 μg/mL streptomycin in a humidified incubator at 37 °C and 5% CO_2, and were seeded in eight-well LabTek chambers (Nunc, Langenselbold, Germany) at a density of 8000 cells per well. Cells were allowed to adhere overnight before they were rinsed 3 times with phosphate buffered saline (PBS). Cell membranes were stained with

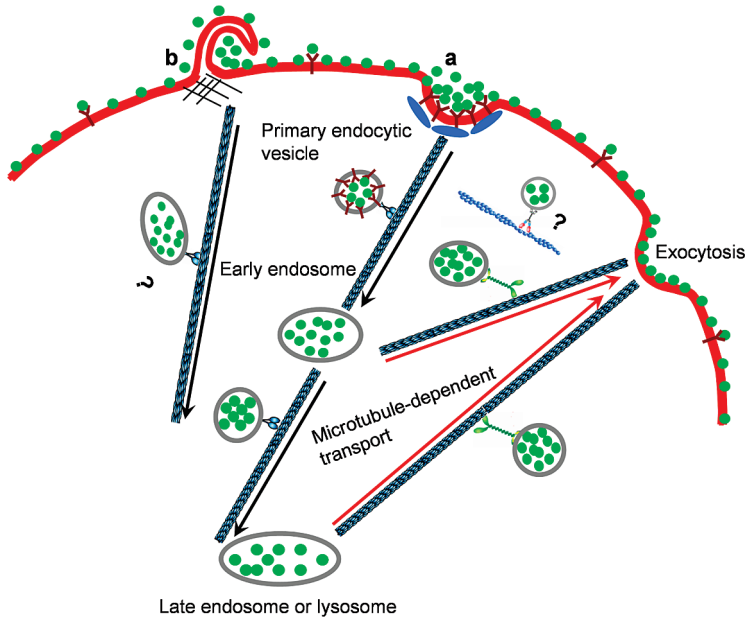

Figure 9. Schematic diagram illustrating the key steps involved in DPA-QD uptake, active transport, and intracellular fate. The uptake process starts with binding of DPA-QDs to the plasma membrane, leading to internalization mainly *via* (a) the clathrin-mediated endocytosis machinery and (b) to a lesser part by macropinocytosis. Clathrin-mediated uptake is followed by active transport of the DPA-QDs, which reside in early endosomes, which develop into late endosomes and finally lysosomes. About half of the internalized DPA-QDs were again exocytosed by the cell.

0.25 μg/mL CellMask Deep Red (Invitrogen, Carlsbad, CA) in PBS for 5 min and washed 3 times with 250 μL of PBS. For nanoparticle uptake experiments, cells were incubated with 250 μL of DPA-QDs at a concentration of 10 nM in PBS by solution exchange unless stated otherwise. The cells were imaged over 1 h in intervals of 3 s using a spinning disk confocal laser microscope assembled from individual components.[47] The instrument is based on an inverted microscope (Axio Observer, Zeiss, Göttingen, Germany) with CO_2 and temperature control (37 °C and 5% CO_2 PECON, Erbach, Germany), four solid-state lasers for excitation (405, 473, 532, and 637 nm), a CSU10 scan head (Yokogawa, Tokyo, Japan), an image splitter unit (OptoSplit II, Cairn Research, Faversham, UK) and an EMCCD camera (DV-887, Andor, Belfast, UK). Images were taken in two spectral channels. Nanoparticles were excited at 532 nm and observed through a bandpass filter (HQ 585/80, AHF, Tübingen, Germany). The red membrane dye was excited at 637 nm, and the emission was filtered through a long-pass (FF01-635/LP, AHF).

Image Analysis. For the quantitative analysis of nanoparticle uptake, we acquired dual-color images of confocal cross sections at about half the cell height. By using custom-written software developed in MATLAB (The MathWorks, Natick, MA), we analyzed the sections as described previously.[13] Briefly, binary masks were generated for both the membrane-associated regions as well as the intracellular space, based on the image of the stained membrane in the red channel. A Sobel filter[48] was used for edge detection before a convex shell was generated around the cell and refined using gradient vector flow fields.[49] Finally, the binary masks of the membrane-associated region and the intracellular space were applied to the green image of the nanoparticles. An average background was subtracted before normalization by the cell's cross-sectional area. To quantify the uptake kinetics, time series were analyzed with the whole-cell mask, correcting each image for its individual background. For the quantitative analyses of nanoparticle uptake within 1 h, shown in the bar graphs, the initial cellular autofluorescence was subtracted.

Inhibitor Studies. Prior to DPA-QD exposure, cells were incubated with an inhibitor solution (80 μM dynasore, 50 μM chlorpromazine, 100 μM EIPA, 5 μM cytochalasin D, or 33 μM nocodazole, all from Sigma-Aldrich) in 250 μL of PBS for 30 min. Afterward, the cells were exposed to a solution containing the same inhibitor concentration plus 10 nM DPA-QDs. Potassium depletion experiments were performed using potassium-free buffer (100 mM NaCl, 50 mM HEPES, pH 7.4).[2,28] After washing the HeLa cells 3 times with 250 μL of hypotonic buffer (potassium-free buffer diluted with water 1:1) and incubation with this solution for 5 min, cells were washed and further incubated with undiluted potassium-free buffer for another 25 min. Finally, the buffer was exchanged for 250 μL of buffer solution containing 10 nM DPA-QDs.

Intracellular Transport Studies. The effect of serum-free environment was studied by incubating HeLa cells with PBS for 0, 1, and 3 h before exchange of the buffer to PBS with 10 nM DPA-QDs. The analysis of intracellular localization and tracking of DPA-QDs was carried out manually using NIH image J software.

Colocalization and Exocytosis Studies. For testing DPA-QD colocalization with endosomes by two-color spinning disk confocal microscopy, cells were incubated with 100 nM AlexaFluor 647-labeled transferrin for 30 min. After 3 times washing with PBS, cells were incubated with 10 nM DPA-QDs for another 40 min prior to imaging. Labeled transferrin was excited at 637 nm and imaged through a FF01-635/LP (AHF) emission filter. Colocalization with lysosomes was examined with cells prepared by incubation with 10 nM DPA-QDs for 30 min, 3 times washing with PBS, and further incubation with 100 nM LysoTracker Green DND 26 (Molecular Probes, Invitrogen) in PBS for 1 h. LysoTracker fluorescence was excited at 473 nm and imaged through an emission filter HQ 502/40 (AHF).

For studies of exocytosis, cells were first incubated with 10 nM DPA-QDs in PBS for 1.5 h to achieve a substantial nanoparticle uptake. Then, the cells were washed 3 times with PBS and supplied with fresh cell medium (DMEM). Series of *z*-stacks with axial distances of 0.2 μm were recorded on the spinning disk confocal microscope using a dwell time of 0.8 s per frame. 3D images were processed and analyzed using the image processing software IMARIS (Bitplane, Zürich, Switzerland). The fraction of exocytosed QDs was calculated from the loss of intracellular fluorescence after solution exchange.

4Pi Confocal Imaging. 4Pi confocal microscopy was performed with a commercial instrument (Leica TCS 4Pi, Leica Microsystems, Mannheim, Germany) to investigate the uptake of DPA-QDs by HeLa cells treated with dynasore or chlorpromazine. Circular quartz coverslips (Leica) were incubated with 1 mL of 50 μg/mL-buffer solution of fibronectin at 37 °C for 1 h. HeLa cells (60000) were grown on modified quartz overnight at 37 °C and

5% CO_2. After serum depletion by 3 times washing with PBS, cells were exposed to dynasore, chlorpromazine, or EIPA in PBS (1 mL each) for 30 min and incubated for another 1 h with 1 mL of inhibitor solution containing 10 nM DPA-QDs. Membranes were stained with 5 μg/mL DiD (Invitrogen) for 1 min by adding DiD from a concentrated stock solution. Cells were fixed with 1 mL of 4% paraformaldehyde dissolved in PBS and postfixed in 1 mL of 50 mM ammonium chloride. After washing twice with PBS, samples were held in a mixture of 90% glycerol in PBS between two quartz coverslips. Dual-color 4Pi images were acquired with two-photon excitation at 850 nm for both the DPA-QDs and the membrane stain DiD; fluorescence was collected through emission filters 535−560 nm and 647−703 nm, respectively. Side-lobe artifacts were removed from the 4Pi images by one-dimensional linear three-point deconvolution using Leica software.

Acknowledgment. This work was supported by the Deutsche Forschungsgemeinschaft (DFG) through the Center for Functional Nanostructures (CFN) and Schwerpunktprogramm 1313, Grant NI291/7.

Supporting Information Available: Nanoparticle characterization (Figure S1) and experimental data on the effect of EIPA on DPA-QD uptake by HeLa cells (Figure S2). This material is available free of charge *via* the Internet at http://pubs.acs.org.

REFERENCES AND NOTES

1. Oberdörster, G.; Oberdörster, E.; Oberdörster, J. Concepts of Nanoparticle Dose Metric and Response Metric. *Environ. Health Perspect.* **2007**, *115*, A290.
2. Subtil, A.; Hemar, A.; Dautry-Varsat, A. Rapid Endocytosis of Interleukin 2 Receptors When Clathrin-Coated Pit Endocytosis Is Inhibited. *J. Cell Sci.* **1994**, *107*, 3461–3468.
3. Conner, S. D.; Schmid, S. L. Regulated Portals of Entry into the Cell. *Nature* **2003**, *422*, 37–44.
4. Nakai, T.; Kanamori, T.; Sando, S.; Aoyama, Y. Remarkably Size-Regulated Cell Invasion by Artificial Viruses. Saccharide-Dependent Self-Aggregation of Glycoviruses and Its Consequences in Glycoviral Gene Delivery. *J. Am. Chem. Soc.* **2003**, *125*, 8465–8475.
5. Osaki, F.; Kanamori, T.; Sando, S.; Sera, T.; Aoyama, Y. A Quantum Dot Conjugated Sugar Ball and Its Cellular Uptake. On the Size Effects of Endocytosis in the Subviral Region. *J. Am. Chem. Soc.* **2004**, *126*, 6520–6521.
6. Cedervall, T.; Lynch, I.; Lindman, S.; Berggard, T.; Thulin, E.; Nilsson, H.; Dawson, K. A.; Linse, S. Understanding the Nanoparticle-Protein Corona Using Methods to Quantify Exchange Rates and Affinities of Proteins for Nanoparticles. *Proc. Natl. Acad. Sci. U.S.A.* **2007**, *104*, 2050–2055.
7. Röcker, C.; Pötzl, M.; Zhang, F.; Parak, W. J.; Nienhaus, G. U. A Quantitative Fluorescence Study of Protein Monolayer Formation on Colloidal Nanoparticles. *Nat. Nanotechnol.* **2009**, *4*, 577–580.
8. Rejman, J.; Oberle, V.; Zuhorn, I. S.; Hoekstra, D. Size-Dependent Internalization of Particles *via* the Pathways of Clathrin- and Caveolae-Mediated Endocytosis. *Biochem. J.* **2004**, *377*, 159–169.
9. Chithrani, B. D.; Chan, W. C. W. Elucidating the Mechanism of Cellular Uptake and Removal of Protein-Coated Gold Nanoparticles of Different Sizes and Shapes. *Nano Lett.* **2007**, *7*, 1542–1550.
10. Chithrani, B. D.; Ghazani, A. A.; Chan, W. C. W. Determining the Size and Shape Dependence of Gold Nanoparticle Uptake into Mammalian Cells. *Nano Lett.* **2006**, *6*, 662–668.
11. Jiang, W.; Kim, B. Y. S.; Rutka, J. T.; Chan, W. C. W. Nanoparticle-Mediated Cellular Response Is Size-Dependent. *Nat. Nanotechnol.* **2008**, *3*, 145–150.
12. Gratton, S. E. A.; Ropp, P. A.; Pohlhaus, P. D.; Luft, J. C.; Madden, V. J.; Napier, M. E.; DeSimone, J. M. The Effect of Particle Design on Cellular Internalization Pathways. *Proc. Natl. Acad. Sci. U.S.A.* **2008**, *105*, 11613–11618.
13. Jiang, X.; Dausend, J.; Hafner, M.; Musyanovych, A.; Röcker, C.; Landfester, K.; Mailänder, V.; Nienhaus, G. U. Specific Effects of Surface Amines on Polystyrene Nanoparticles in Their Interactions with Mesenchymal Stem Cells. *Biomacromolecules* **2010**, *11*, 748–753.
14. Ryman-Rasmussen, J. P.; Riviere, J. E.; Monteiro-Riviere, N. A. Variables Influencing Interactions of Untargeted Quantum Dot Nanoparticles with Skin Cells and Identification of Biochemical Modulators. *Nano Lett.* **2007**, *7*, 1344–1348.
15. Delehanty, J. B.; Medintz, I. L.; Pons, T.; Brunel, F. M.; Dawson, P. E.; Mattoussi, H. Self-Assembled Quantum Dot−Peptide Bioconjugates for Selective Intracellular Delivery. *Bioconjugate Chem.* **2006**, *17*, 920–927.
16. Silver, J.; Ou, W. Photoactivation of Quantum Dot Fluorescence Following Endocytosis. *Nano Lett.* **2005**, *5*, 1445–1449.
17. Chan, W. C. W.; Maxwell, D. J.; Gao, X.; Bailey, R. E.; Han, M.; Nie, S. Luminescent Quantum Dots for Multiplexed Biological Detection and Imaging. *Curr. Opin. Biotechnol.* **2002**, *13*, 40–46.
18. Michalet, X.; Pinaud, F. F.; Bentolila, L. A.; Tsay, J. M.; Doose, S.; Li, J. J.; Sundaresan, G.; Wu, A. M.; Gambhir, S. S.; Weiss, S. Quantum Dots for Live Cells, *in Vivo* Imaging, and Diagnostics. *Science* **2005**, *307*, 538–544.
19. Bruchez, M., Jr.; Moronne, M.; Gin, P.; Weiss, S.; Alivisatos, A. P. Semiconductor Nanocrystals as Fluorescent Biological Labels. *Science* **1998**, *281*, 2013–2016.
20. Chan, W. C. W.; Nie, S. Quantum Dot Bioconjugates for Ultrasensitive Nonisotopic Detection. *Science* **1998**, *281*, 2016–2018.
21. Lidke, D. S.; Nagy, P.; Heintzmann, R.; Arndt-Jovin, D. J.; Post, J. N.; Grecco, H. E.; Jares-Erijman, E. A.; Jovin, T. M. Quantum Dot Ligands Provide New Insights into Erbb/Her Receptor-Mediated Signal Transduction. *Nat. Biotechnol.* **2004**, *22*, 198–203.
22. Cambi, A.; Lidke, D. S.; Arndt-Jovin, D. J.; Figdor, C. G.; Jovin, T. M. Ligand-Conjugated Quantum Dots Monitor Antigen Uptake and Processing by Dendritic Cells. *Nano Lett.* **2007**, *7*, 970–977.
23. Sundara Rajan, S.; Vu, T. Q. Quantum Dots Monitor Trka Receptor Dynamics in the Interior of Neural Pc12 Cells. *Nano Lett.* **2006**, *6*, 2049–2059.
24. Courty, S.; Luccardini, C.; Bellaiche, Y.; Cappello, G.; Dahan, M. Tracking Individual Kinesin Motors in Living Cells Using Single Quantum-Dot Imaging. *Nano Lett.* **2006**, *6*, 1491–1495.
25. Klostranec, J. M.; Chan, W. C. W. Quantum Dots in Biological and Biomedical Research: Recent Progress and Present Challenges. *Adv. Mater.* **2006**, *18*, 1953–1964.
26. Breus, V. V.; Heyes, C. D.; Nienhaus, G. U. Quenching of CdSe−ZnS Core−Shell Quantum Dot Luminescence by Water-Soluble Thiolated Ligands. *J. Phys. Chem. C* **2007**, *111*, 18589–18594.
27. Breus, V. V.; Heyes, C. D.; Tron, K.; Nienhaus, G. U. Zwitterionic Biocompatible Quantum Dots for Wide Ph Stability and Weak Nonspecific Binding to Cells. *ACS Nano* **2009**, *3*, 2573–2580.
28. Rejman, J.; Bragonzi, A.; Conese, M. Role of Clathrin- and Caveolae-Mediated Endocytosis in Gene Transfer Mediated by Lipo- and Polyplexes. *Mol. Ther.* **2005**, *12*, 468–474.
29. Stuart, A. D.; Brown, T. D. K. Entry of Feline Calicivirus Is Dependent on Clathrin-Mediated Endocytosis and Acidification in Endosomes. *J. Virol.* **2006**, *80*, 7500–7509.
30. Dausend, J.; Musyanovych, A.; Dass, M.; Walther, P.; Schrezenmeier, H.; Landfester, K.; Mailänder, V. Uptake Mechanism of Oppositely Charged Fluorescent Nanoparticles in Hela Cells. *Macromol. Biosci.* **2008**, *8*, 1135–1143.
31. Brodsky, F. M.; Chen, C.-Y.; Knuehl, C.; Towler, M. C.; Wakeham, D. E. Biological Basket Weaving: Formation and Function of Clathrin-Coated Vesicles. *Annu. Rev. Cell Dev. Biol.* **2001**, *17*, 517–568.

32. Harush-Frenkel, O.; Debotton, N.; Benita, S.; Altschuler, Y. Targeting of Nanoparticles to the Clathrin-Mediated Endocytic Pathway. *Biochem. Biophys. Res. Commun.* **2007**, *353*, 26–32.
33. Harush-Frenkel, O.; Rozentur, E.; Benita, S.; Altschuler, Y. Surface Charge of Nanoparticles Determines Their Endocytic and Transcytotic Pathway in Polarized Mdck Cells. *Biomacromolecules* **2008**, *9*, 435–443.
34. Anas, A.; Okuda, T.; Kawashima, N.; Nakayama, K.; Itoh, T.; Ishikawa, M.; Biju, V. Clathrin-Mediated Endocytosis of Quantum Dot-Peptide Conjugates in Living Cells. *ACS Nano* **2009**, *3*, 2419–2429.
35. Ruan, G.; Agrawal, A.; Marcus, A. I.; Nie, S. Imaging and Tracking of Tat Peptide-Conjugated Quantum Dots in Living Cells: New Insights into Nanoparticle Uptake, Intracellular Transport, and Vesicle Shedding. *J. Am. Chem. Soc.* **2007**, *129*, 14759–14766.
36. Macia, E.; Ehrlich, M.; Massol, R.; Boucrot, E.; Brunner, C.; Kirchhausen, T. Dynasore, a Cell-Permeable Inhibitor of Dynamin. *Dev. Cell* **2006**, *10*, 839–850.
37. Wang, L. H.; Rothberg, K. G.; Anderson, R. G. Mis-assembly of Clathrin Lattices on Endosomes Reveals a Regulatory Switch for Coated Pit Formation. *J. Cell Biol.* **1993**, *123*, 1107–1117.
38. Ivanchenko, S.; Glaschick, S.; Röcker, C.; Oswald, F.; Wiedenmann, J.; Nienhaus, G. U. Two-Photon Excitation and Photoconversion of Eosfp in Dual-Color 4pi Confocal Microscopy. *Biophys. J.* **2007**, *92*, 4451–4457.
39. Gekle, M.; Drumm, K.; Mildenberger, S.; Freudinger, R.; Gaβner, B.; Silbernagl, S. Inhibition of Na^+-H^+ Exchange Impairs Receptor-Mediated Albumin Endocytosis in Renal Proximal Tubule-Derived Epithelial Cells from Opossum. *J. Physiol.* **1999**, *520*, 709–721.
40. Gekle, M.; Freudinger, R.; Mildenberger, S. Inhibition of Na^+-H^+ Exchanger-3 Interferes with Apical Receptor-Mediated Endocytosis *via* Vesicle Fusion. *J. Physiol.* **2001**, *531*, 619–629.
41. King, S. J.; Schroer, T. A. Dynactin Increases the Processivity of the Cytoplasmic Dynein Motor. *Nat. Cell Biol.* **2000**, *2*, 20–24.
42. Nan, X.; Sims, P. A.; Chen, P.; Xie, X. S. Observation of Individual Microtubule Motor Steps in Living Cells with Endocytosed Quantum Dots. *J. Phys. Chem. B* **2005**, *109*, 24220–24224.
43. Levi, V.; Serpinskaya, A. S.; Gratton, E.; Gelfand, V. Organelle Transport Along Microtubules in Xenopus Melanophores: Evidence for Cooperation between Multiple Motors. *Biophys. J.* **2006**, *90*, 318–327.
44. Qualmann, B.; Kessels, M. M.; Kelly, R. B. Molecular Links between Endocytosis and the Actin Cytoskeleton. *J. Cell Biol.* **2000**, *150*, F111–116.
45. Nel, A. E.; Madler, L.; Velegol, D.; Xia, T.; Hoek, E. M. V.; Somasundaran, P.; Klaessig, F.; Castranova, V.; Thompson, M. Understanding Biophysicochemical Interactions at the Nano-Bio Interface. *Nat. Mater.* **2009**, *8*, 543–557.
46. Gao, H.; Shi, W.; Freund, L. B. Mechanics of Receptor-Mediated Endocytosis. *Proc. Natl. Acad. Sci. U.S.A.* **2005**, *102*, 9469–9474.
47. Jiang, X.; Weise, S.; Hafner, M.; Röcker, C.; Zhang, F.; Parak, W. J.; Nienhaus, G. U. Quantitative Analysis of the Protein Corona on Fept Nanoparticles Formed by Transferrin Binding. *J. R. Soc. Interface* **2010**, *7*, S5–S13.
48. Duda, R. O.; Hart, P. E. In *Pattern Classification and Scene Analysis*; John Wiley and Sons: New York, 1973; pp 271−272.
49. Xu, C.; Prince, J. L. Snakes, Shapes, and Gradient Vector Flow. *IEEE Trans. Image Process.* **1998**, *7*, 359–369.